PNAS
www.pnas.org

Supplementary Information for

Replication is the key barrier during the dual-host adaption of mosquito-borne flaviviruses

Yanan Zhang[†1,3], Dening Liang[†2], Fei Yuan[1], Yiran Yan[1,3], Zuoshu Wang[4], Pan Liu[2], Qi Yu[2], Xing Zhang[5], Xiangxi Wang[*2], Aihua Zheng[*1,3,6]

* Corresponding authors: Xiangxi Wang, Aihua Zheng
Email: xiangxi@ibp.ac.cn (X. W.); zhengaihua@ioz.ac.cn (A. Z.).

This PDF file includes:

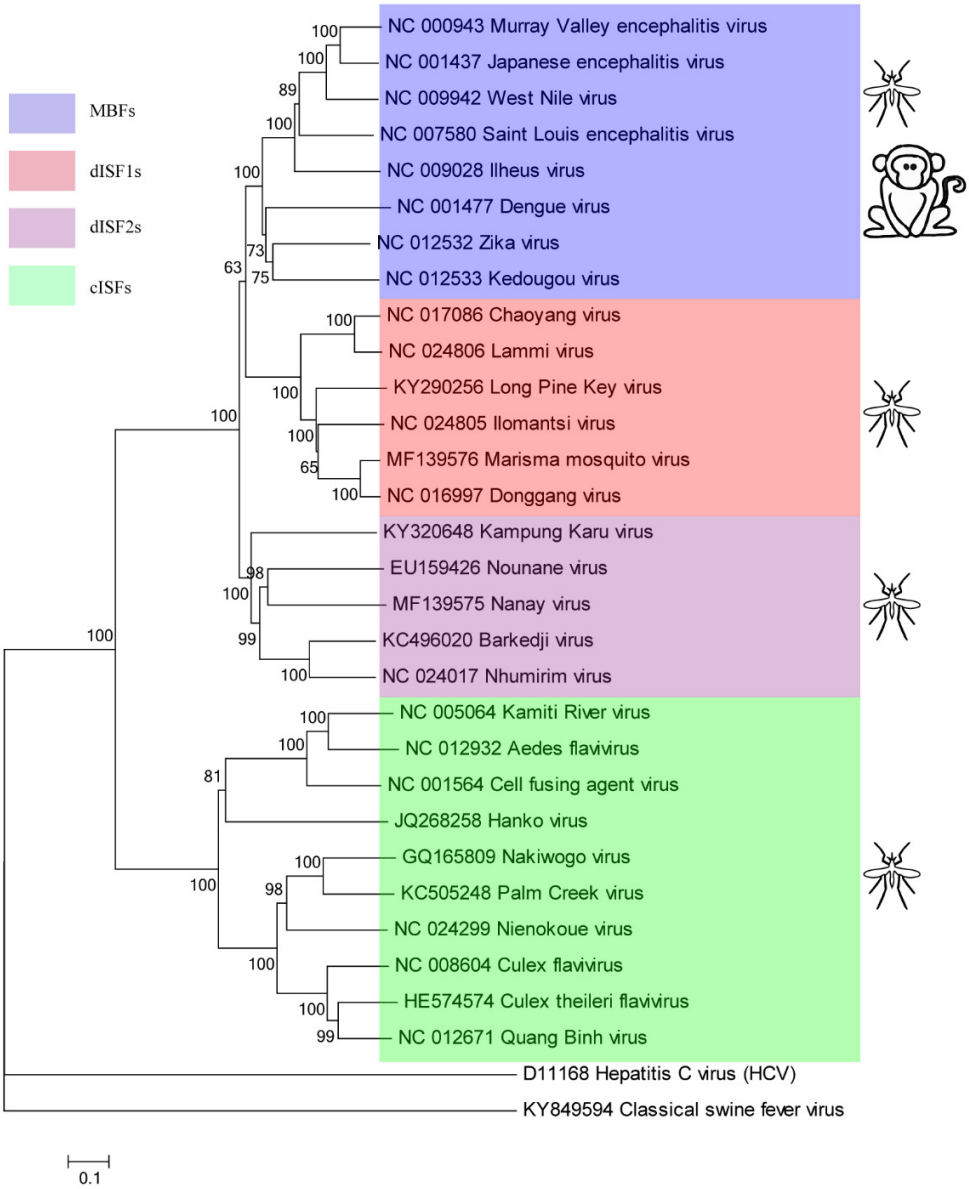

Supplementary figure1. Phylogenetic tree of different groups of flaviviruses introducing Hepatitis C virus and classical swine fever virus as the outgroup. Complete polyprotein amino acid sequences were aligned and a maximum likelihood phylogenetic tree was reconstructed in MEGA7(1). The consensus tree inferred based on 500 replicates (2) is taken to represent the evolutionary history of the taxa, where the bootstrap values are shown along the branch. Highlighted in blue are mosquito-borne flaviviruses (MBFs), red are dual-host affiliated insect-specific flaviviruses 1 (dISF1s), purple are dual-host affiliated insect-specific flaviviruses 2 (dISF2s), and green are classical insect-specific flaviviruses (cISFs).

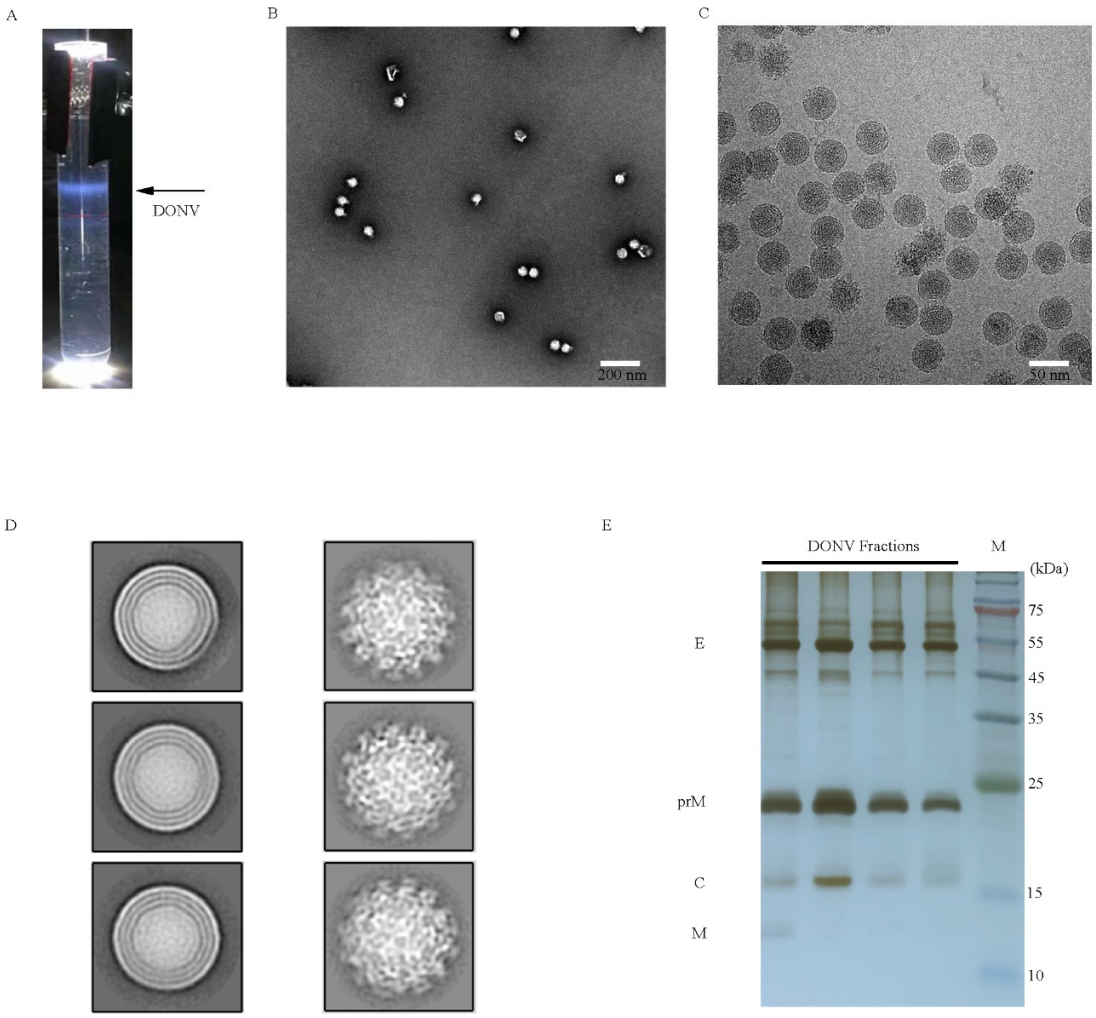

Supplementary Figure 2. Purification and data collection of DONV. (A) Zonal ultracentrifugation of a 15–45% (w/v) sucrose density gradient at 30,000 rpm for 3 h was used to purify DONV from the harvest concentrate described in the Methods section. (B) The negative-stain images of DONV. (C) The cryo-EM micrograph of DONV. (D) Representative classes from 2D classification in RELION for DONV. (E) SDS-PAGE analysis of continuous sucrose gradient ultracentrifugation purified DONV virions followed by silver staining.

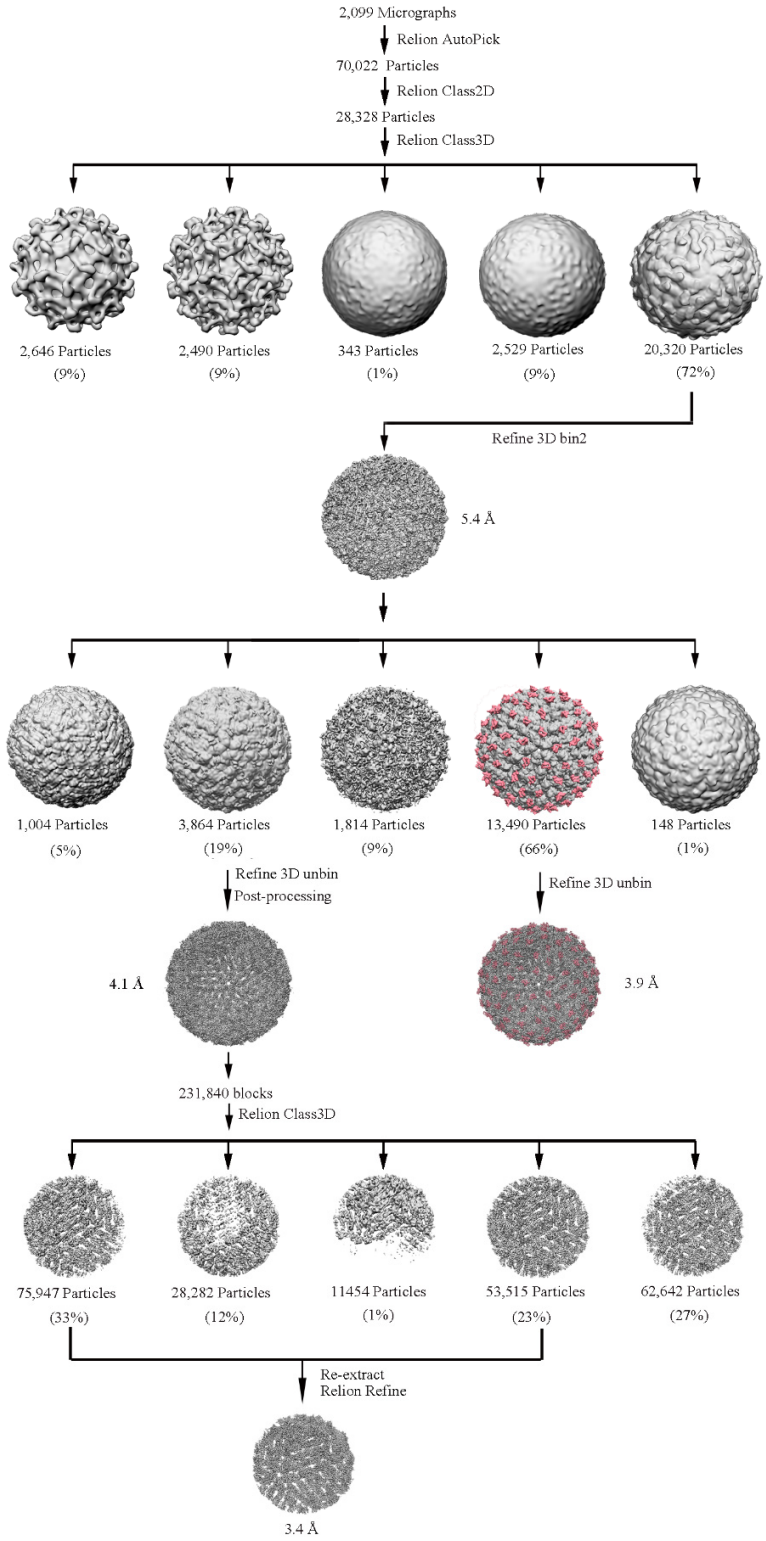

Supplementary Figure 3. Flow-chart for Cryo-EM data processing. The data processing procedures for DONV. Details are given in the Methods section.

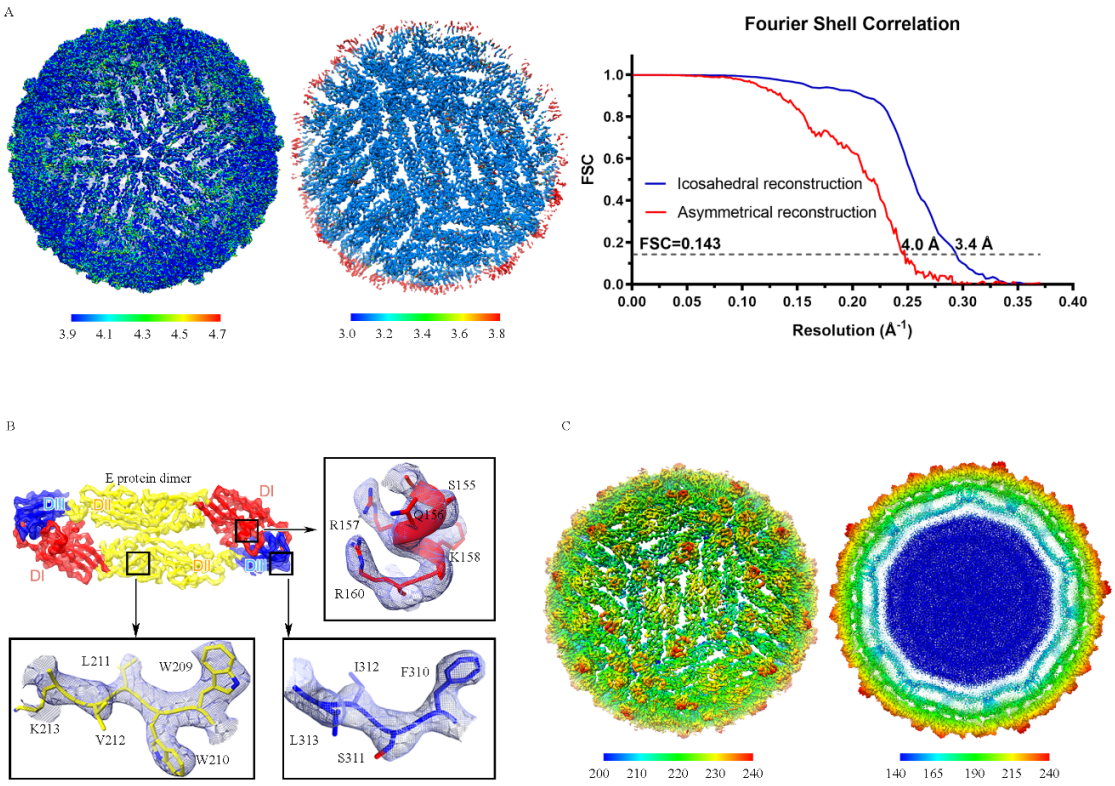

Supplementary Figure 4. Assessment of resolution and electron density maps. (A) The map resolution assessment of icosahedral and asymmetrical reconstructions, showing resolutions distribution from 3.9 to 4.7 Å and 3.0 to 3.8 Å. The gold-standard FSC curves of icosahedral and asymmetrical reconstructions. The resolutions at FSC=0.143 are 4.0 Å and 3.4 Å. (B) Electron density maps for a section of the envelope protein DI, DII, and DIII domain. (C) Cryo-EM map of DONV viewed down an icosahedral twofold axis.

Supplementary Figure 5. Sequence alignment of viruses shown in figure 1. (A) Alignment of E protein sequences of DONV with WNV, ZIKV, and JEV. DI, DII, DIII, and stem (H1, H2, H3, T1, and T2) are indicated below the sequences and shown in red, yellow, blue, and cyan, respectively. The secondary structures of DONV are labeled above the sequences. (B) Sequence alignment of E proteins glycosylation motif from representative dISFs and MBFs. Potential N-glycosylation site amin acid 153/154 is labeled with asterisk.

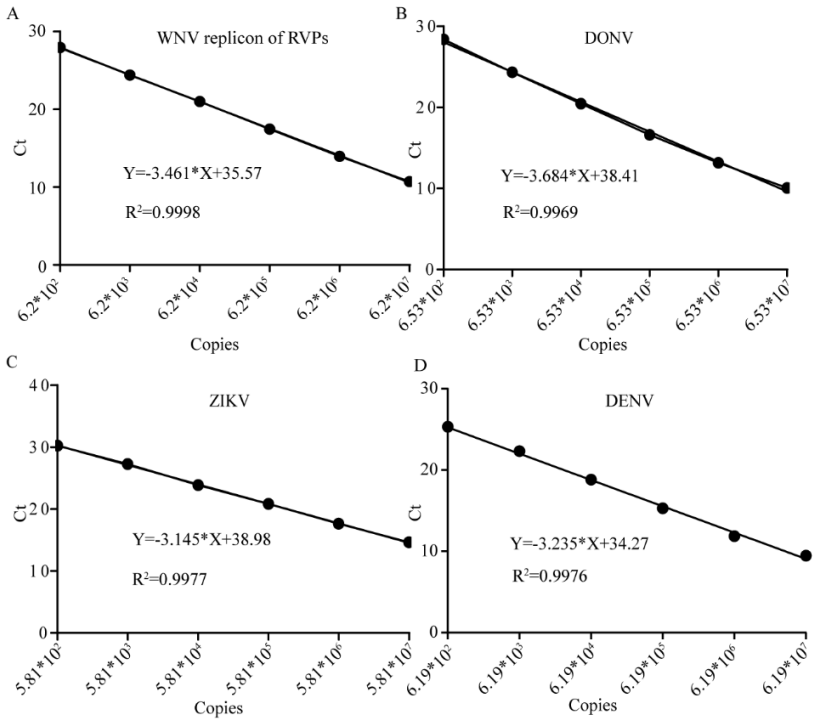

Supplementary Figure 6. Standard curve for the real-time PCR assays for the detection of WNV replicon in the RVPs (A), DONV (B), ZIKV (C), and DENV (D). The sizes of the PCR products are 105 bp, 132 bp, 122 bp, and 143 bp for WNV replicon, DONV, ZIKV, and DENV, respectively. The correlation coefficients (R^2) were 0.9998, 0.9969, 0.9977, and 0.9976 for WNV (A), DONV (B), ZIKV (C), and DENV (D), respectively. The linear dynamic ranges of both assays were higher than 6 logs, and all the threshold cycle (Ct) values in the following experiments fell into the dynamic ranges. The results represent two independent experiments.

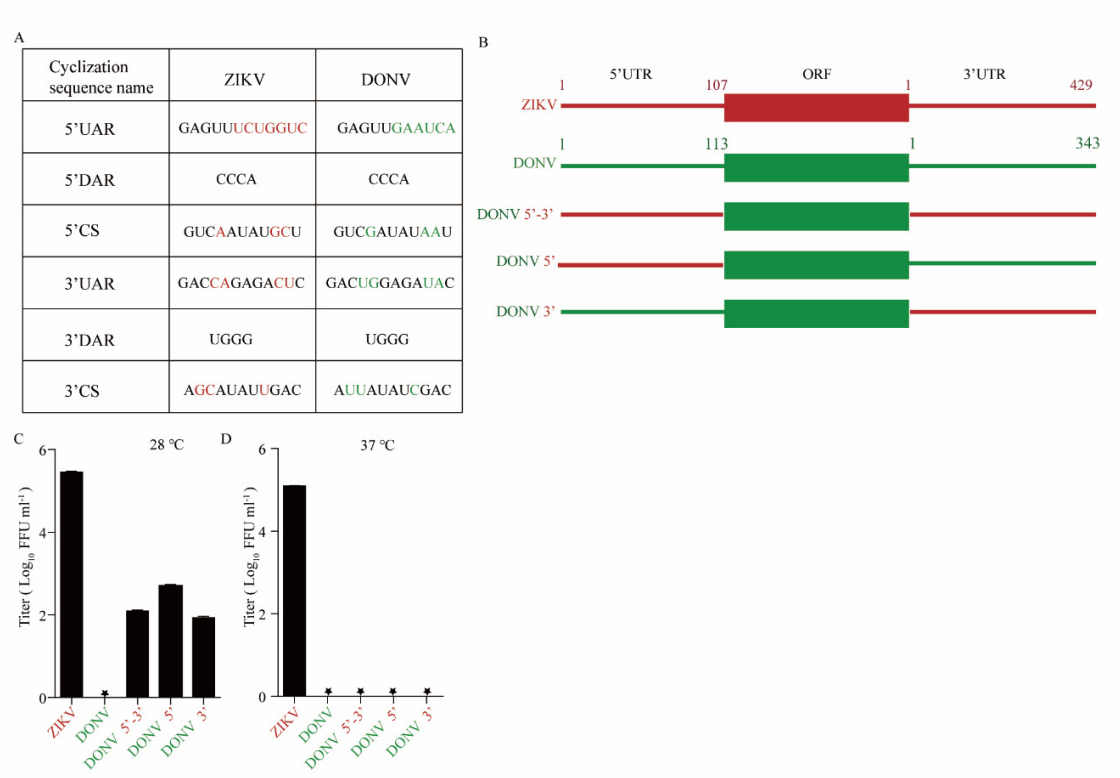

Supplementary Figure 7. Release of DONV 5', DONV 3', and DONV 5'-3' was partially rescued at 28 ℃. (A) Cyclization sequences of ZIKV and DONV. (B) Schematic diagram of chimeric infectious clones. DONV 5'-3', the UTRs of DONV replaced by those of ZIKV; DONV 5', the 5' UTR of DONV replaced by ZIKV; DONV 3', the 3' UTR of DONV replaced by ZIKV. (C and D) ZIKV, DONV, and chimeric infectious clones were transfected into 293T cells. The titers of viruses in the supernatants at 28 ℃ and 37 ℃ were tested by a focus-forming assay. n=3. Error bars indicate SD. These results represent three independent experiments.

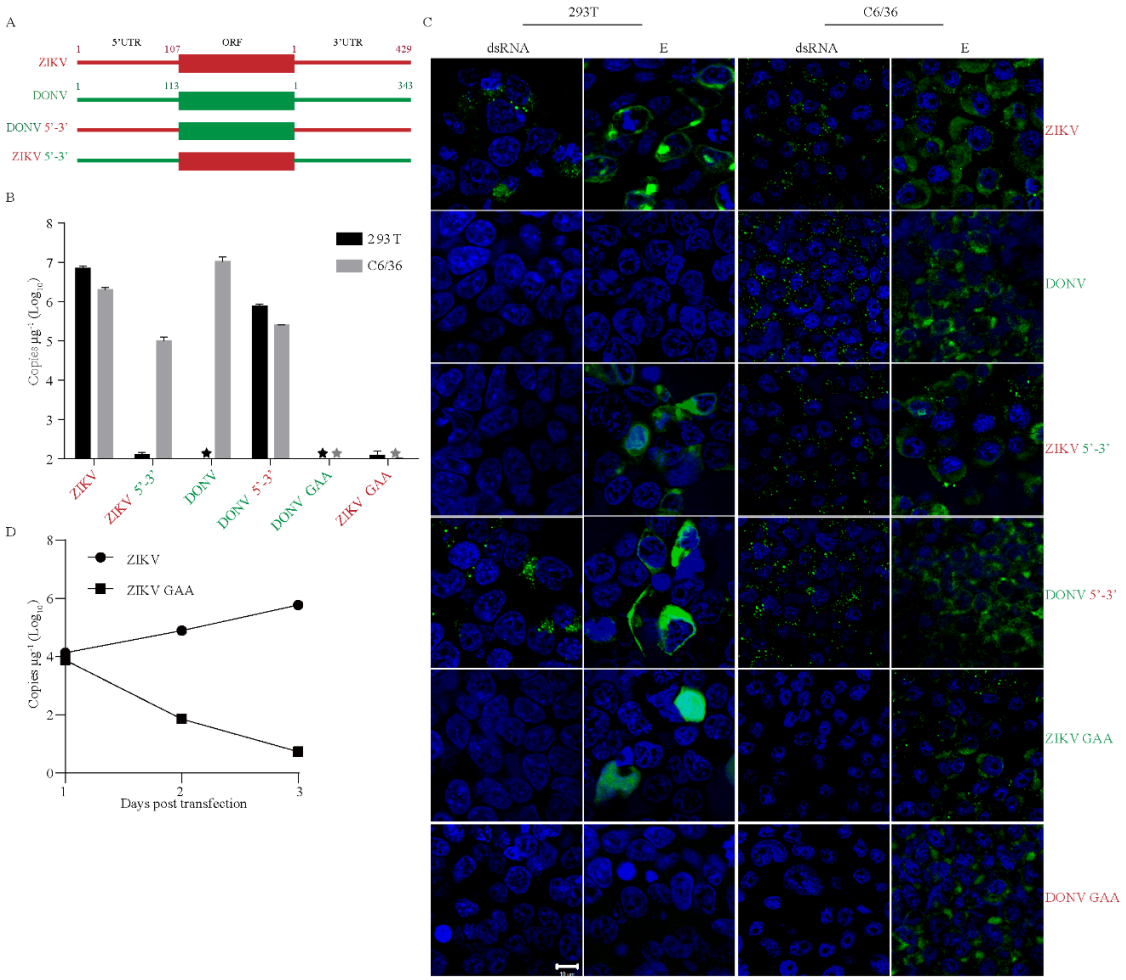

Supplementary Figure 8. Replacement of ZIKV UTRs with those of DONV abolished ZIKV replication in vertebrate cells. (A) Schematic diagram of chimeric infectious clones. DONV 5'-3', the UTRs of DONV replaced by those of ZIKV; ZIKV 5'-3', the UTRs of ZIKV replaced by those of DONV. (B) Viral RNA replication of WT and chimeric viruses in vertebrate cells and C6/36 cells as measured by real-time PCR. n=3. Error bars indicate SD. (C) Immunofluorescence analysis of viral double-strand RNA by anti-dsRNA mAb and envelop protein E by 4G2 mAb of chimeric infectious clones in transfected human 293T cells and mosquito C6/36 cells. (D) The viral RNA levels of GAA mutants in 293T cells in (B) as measured at different time-points. WT and GAA ZIKV infectious clones were transfected into 293T cells and viral RNAs were measured by real-time PCR at indicated time-points. These results represent three independent experiments.

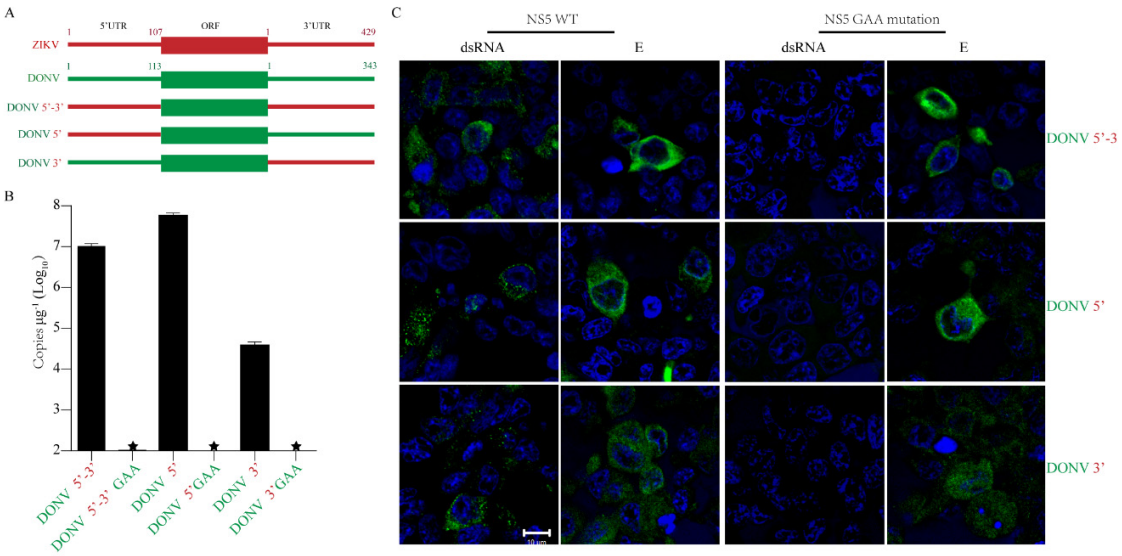

Supplementary Figure 9. GAA mutation in the NS5 protein abolished the replication of DONV 5', DONV 3', and DONV 5'-3' without affecting viral protein translation in 293T cells. **(**A) Schematic diagram of chimeric infectious clones. (B) 293T cells were transfected with the infectious clones of viruses with WT or GAA mutant NS5. Replication of viruses in 293T cell lysates were measured by real-time PCR 48 h later. n=3.Error bars indicate SD. (C) Double-strand RNA (dsRNA) and E protein were detected by immunofluorescence with mAb against dsRNA and 4G2 respectively (green). Nuclei were stained by Hoechst 33342 (blue). These results represent three independent experiments.

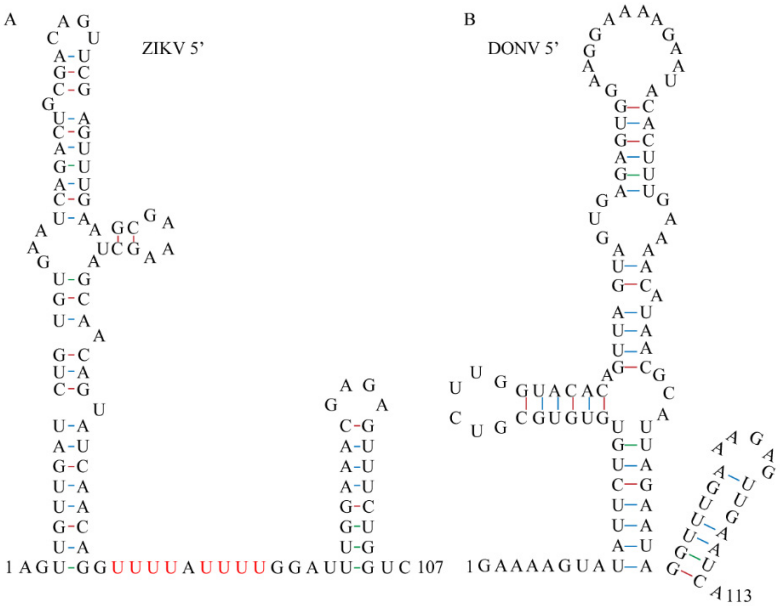

Supplementary Figure 10. Predicted secondary structure of ZIKV (A) and DONV 5' UTR (B) by RNAfold.

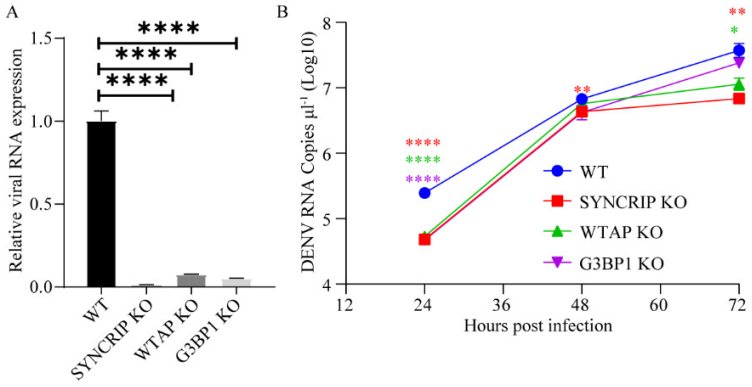

Supplementary Figure 11. WTAP, SYNCRIP, and G3BP1 are critical for DENV replication in 293T cells. (A) Viral RNA replication in WT, WTAP-KO (knockout), G3BP1-KO, and SYNCRIP-KO cells. The cells were infected with DENV at an MOI of 0.1. RNAs were isolated by Trizol reagent 72 h post infection and tested by real-time PCR. The expression of Viral RNA was normalized to relative to β-actin. The value of WT was set as 1. (B) Viral RNA in the supernatants of WT, WTAP-KO, G3BP1-KO, and SYNCRIP-KO cells at indicated times were tested by real-time PCR. The data was analyzed by unpaired *t* test (A) and multiple *t* test (B). n=3. Error bars indicate SD. These results represent three independent experiments.

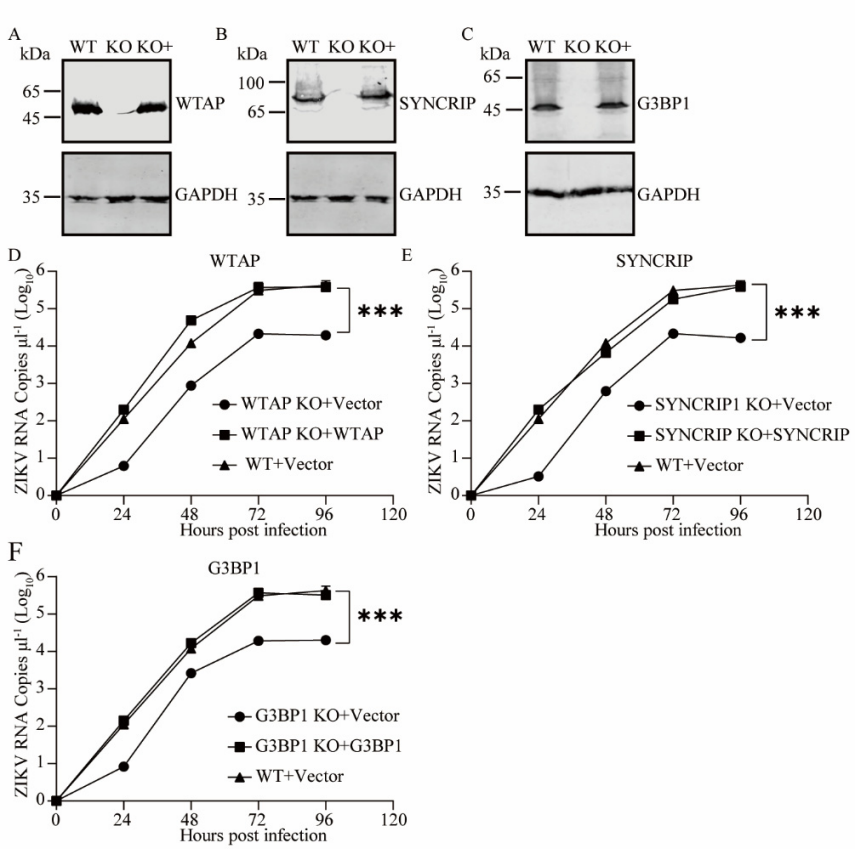

Supplementary Figure 12. WTAP, SYNCRIP, and G3BP1 are critical for ZIKV replication in 293T cells. The expressions of WTAP (A), SYNCRIP (B), and G3BP1 (C) in WT, knockout (KO), and knockout+transduction (KO+) 293T cells were tested by Western blot with mAbs against indicated proteins. (D-F) WT, KO, and KO+ 293T cell lines were infected by ZIKV at an MOI of 0.1. Viral RNA in the supernatants was measured by real-time PCR at indicated times. The data was analyzed by multiple t test. n=3 and error bars indicate SD. The results represent three independent experiments.

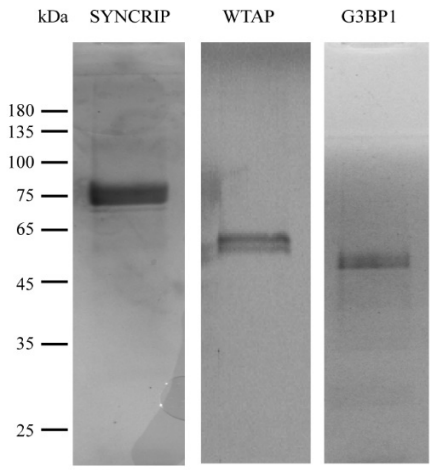

Supplementary Figure 13. The Coomassie Blue staining of the purified proteins.

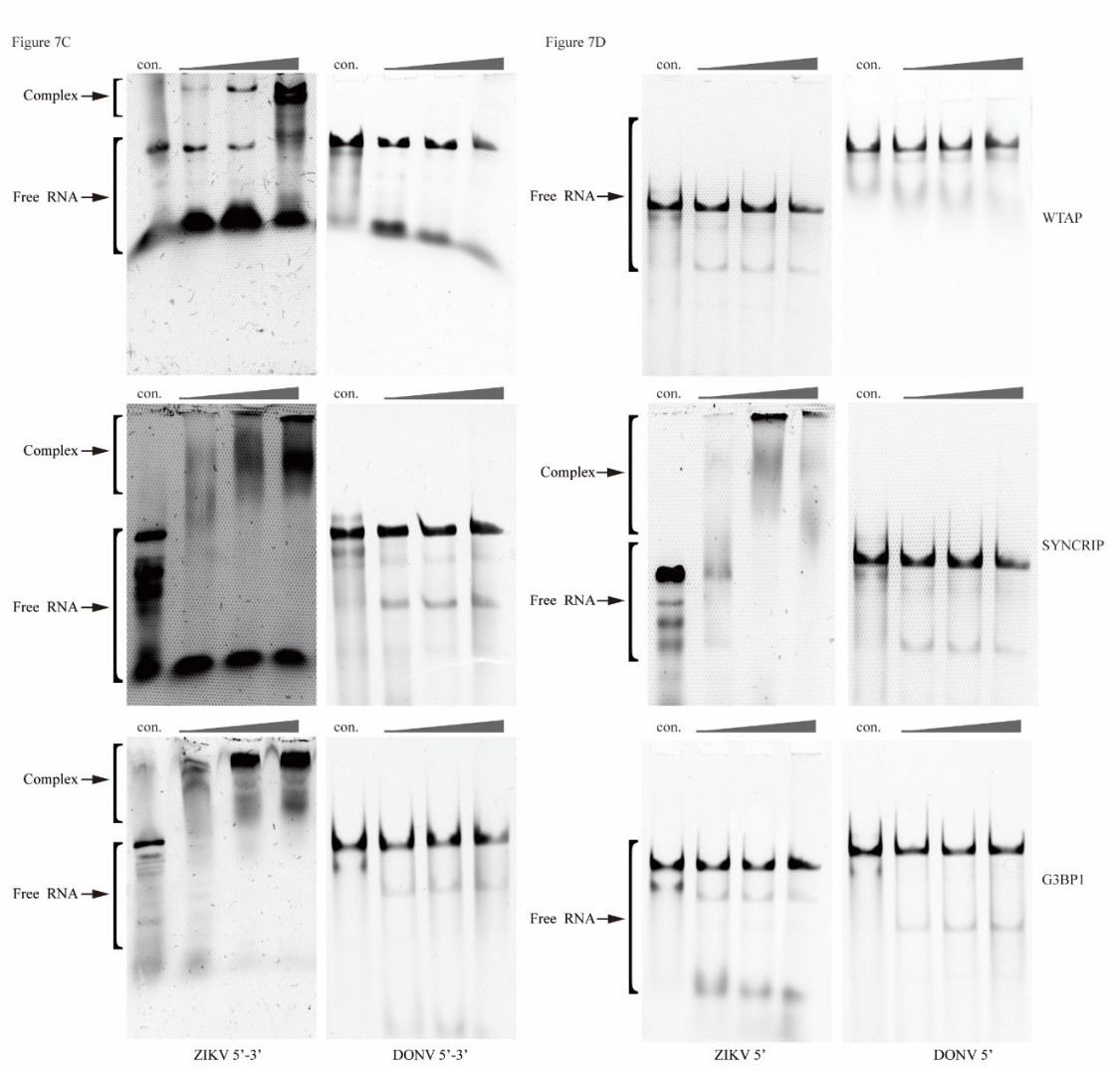
Figure 7C
Figure 7D
con.
Complex
Free RNA
WTAP
SYNCRIP
G3BP1
ZIKV 5'-3'
DONV 5'-3'
ZIKV 5'
DONV 5'

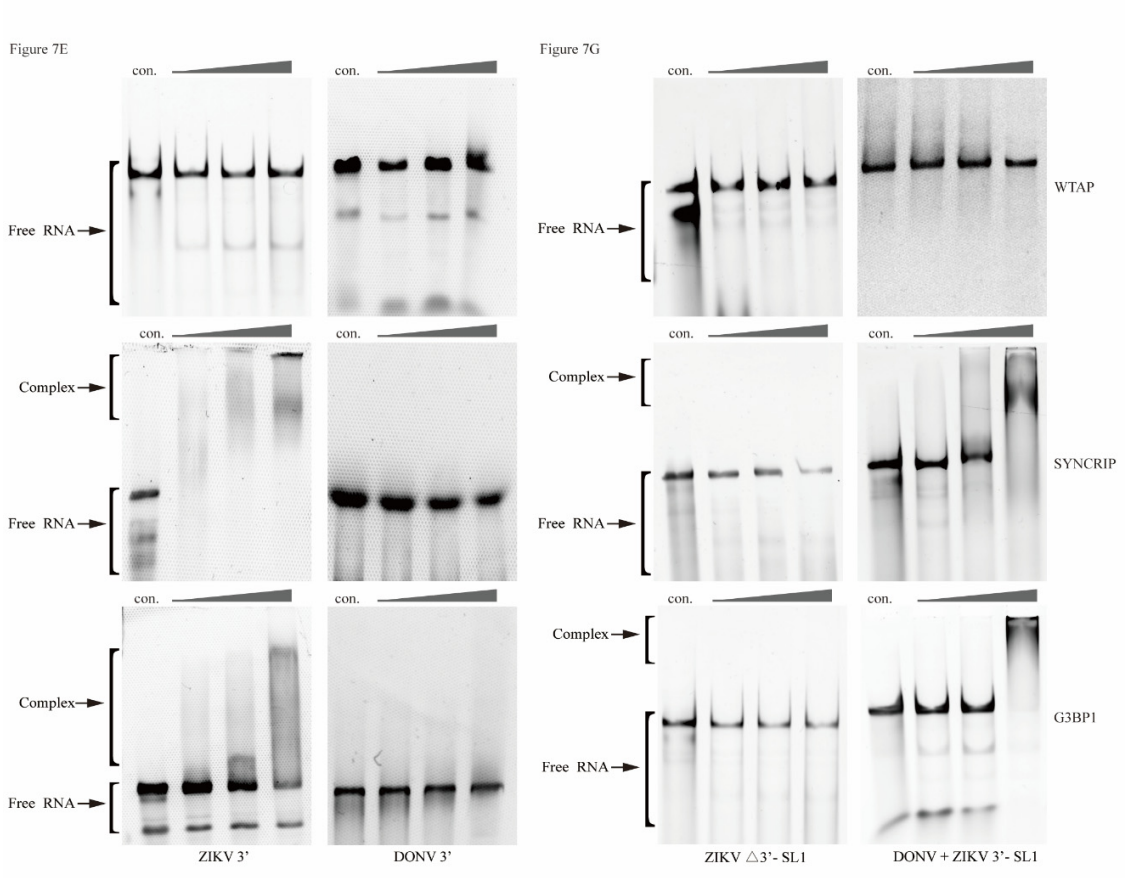

Supplementary Figure 14. Original images of EMSA in Figure 7. Panels are labeled according to Figure 7.

Supplementary Table 1 Cryo-EM data collection and processing statistics.

	Smooth DONV viron	**Smooth DONV asymmetric unit**	**Spiky DONV viron**
Microscope	FEI Tecnai G2 Polara	FEI Tecnai G2 Polara	FEI Tecnai G2 Polara
Detector	Gatan K2 Summit	Gatan K2 Summit	Gatan K2 Summit
Voltage (kV)	300	300	300
Recording mode	Super resolution	Super resolution	Super resolution
Electron exposure ($e^-/Å^2$)	35	35	35
Spherical aberration (mm)	2.7	2.7	2.7
Defocus range (μm)	1.5-2.5	1.5-2.5	1.5-2.5
Magnification	105,000	105,000	105,000
Movie pixel size (Å)	0.675	0.675	0.675
Final map pixel size (Å)	1.35	1.35	1.35
Micrographs total	2,099	2,099	2,099
Micrographs used	2,099	2,099	2,099
Initial particle images	20,320	231,840	5,136
Final particle images	3,864	129,462	
Symmetry imposed	I3	C1	
Map sharpening B factors ($Å^2$)	-107	-41	--
Map resolution (FSC 0.5 cut-off)	4.6	3.9	
Map resolution (FSC 0.143 cut-off)	4.1	3.4	

Supplementary Table 2 Model refinement statistics.

Initial model used (PDB code)	6CO8
R.M.S.D	
Bond lengths (Å)	0.007
Bond angles (°)	0.821
Validation	
MolProbity score	2.08
Clashscore	10.70
Rotamer outliers (%)	0.00
Cβ outliers (%)	0.00
Ramachandran plot	
Favored	90.48
Allowed	9.52
Disallowed	0.00

Supplementary References

1. Kumar S, Stecher G, & Tamura K (2016) MEGA7: Molecular Evolutionary Genetics Analysis Version 7.0 for Bigger Datasets. *Mol Biol Evol* 33(7):1870-1874.
2. Felsenstein J (1985) CONFIDENCE LIMITS ON PHYLOGENIES: AN APPROACH USING THE BOOTSTRAP. *Evolution; international journal of organic evolution* 39(4):783-791.